Sensitivity analysis of a coupled plasmonic problem*

Ahmad H. Bokhari†, Eddie Wadbro‡

Abstract

In material distribution-based topology optimization, we place material inside a design domain to extremize an objective function. The optimization problem is solved using a gradient-based algorithm. An efficient way to compute the gradients is to use the adjoint method. This study performs the sensitivity analysis of a coupled plasmonic problem using the adjoint method. More precisely, a TE-polarized Helmholtz equation is coupled to a Poisson equation. The sensitivity analysis of the coupled plasmonic problem poses some challenges stemming from the complex solution of the plasmonic problem. Therefore, we first consider a model problem whose structure is similar to the main problem in some ways but is simpler to study. After examining the model problem, we perform the sensitivity analysis of the coupled plasmonic problem, highlighting key differences between the two problems.

Keywords: metallic antenna; plasmonics; sensitivity analysis; adjoint method; material distribution

1 Introduction

Nanotechnology has enabled the development of novel nano-devices that can take advantage of the advanced technological abilities of magnetic and electric systems. Plasmonics is a rapidly growing field of nanotechnology. Metals such

*Technical Report UMINF 22.04. ISSN 0348-0542

†Department of Computing Science, Umeå University, SE-901 87 Umeå, Sweden, email: ahmadb@cs.umu.se

‡Department of Computing Science, Umeå University, SE-901 87 Umeå, Sweden. Department of Mathematics and Computer Science, Karlstad University, SE-651 88 Karlstad, Sweden, eddie.wadbro@kau.se

as gold or silver are used in plasmonics to design metallic nano-antennas that concentrate electromagnetic energy. Such antennas have applications in cancer treatment [7], lithography [13], and communication [16, 24]. Here, we study a metallic nano-antenna that raises the average temperature in a small region by concentrating the electromagnetic energy. The target application is photo-thermal therapy [4,14]. For the mathematical modeling of this device, we consider a coupled plasmonic problem where a TE-polarized Helmholtz equation is coupled to a Poisson equation. The quantity of interest is the temperature in a target region. In this study, we perform the sensitivity analysis of this coupled system for the topology optimization problem.

Material distribution-based topology optimization uses a material indicator function to model the presence and absence of material inside the design domain. This technique has been successfully applied in many fields for designing systems involving structures [1,8,18,25], fluid flow [6,23], acoustics [5,10,17,20], microwave [2,3,11,12], and plasmonics [9,15,21]. Most commonly, a gradient-based algorithm like the method of moving asymptotes (MMA) [19] is employed to solve the optimization problem. This study performs the sensitivity analysis using the adjoint method and verifies it using the finite difference method. We first consider a model problem involving the coupling of two Poisson equations. It is easier to perform the sensitivity analysis on the model problem because we avoid the complex solution of the TE-polarized Helmholtz equation by only considering the Poisson–Poisson coupling. The model problem aids in the understanding of the main problem. Hence, after studying the model problem, we perform the sensitivity analysis of the coupled plasmonic problem and highlight key differences.

2 Problem description

We consider time harmonic electromagnetic wave propagation governed by the following Maxwell's equation

$$\nabla \times \left(\frac{1}{\epsilon} \nabla \times \boldsymbol{H} \right) - k^2 \boldsymbol{H} = 0, \tag{1}$$

where $\boldsymbol{H}$ is the magnetic field, ϵ is the relative permittivity, the wave number $k = \omega/c$, ω is the angular frequency, $c = 1/(\mu_0 \epsilon_0)^{1/2}$ is the speed of light, in which μ_0 and ϵ_0 denote the permeability and permittivity in free space, respectively.

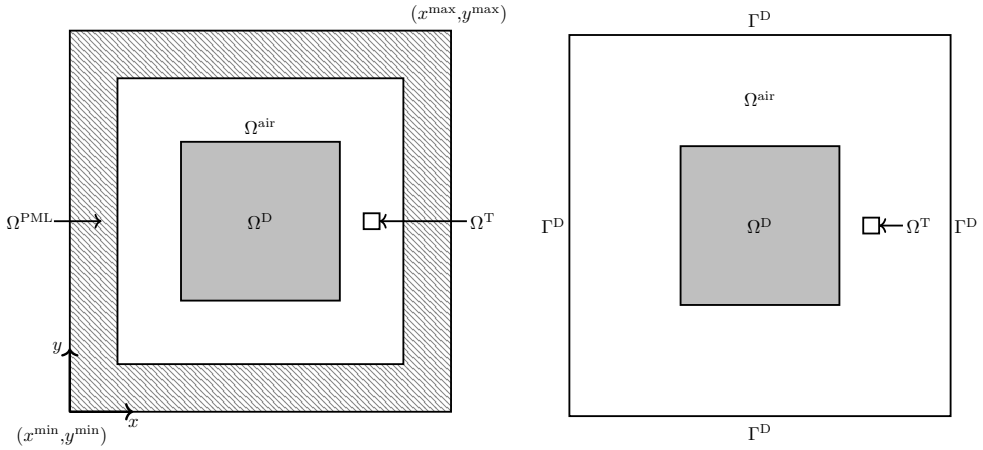

Figure 1: Left: Computational domain for the plasmonic problem Ω. Right: Computational domain for the Poisson problem Ω.

We assume that the waves are TE-polarized. That is, we use $\boldsymbol{H} = (0, 0, u)$, which reduces Eq. (1) to two-dimensional Helmholtz equation

$$-\nabla \cdot \left(\frac{1}{\epsilon}\nabla u\right) - k^2 u = 0. \tag{2}$$

In addition, we assume that the total field u is a combination of incoming and outgoing waves

$$u = u^{\text{in}} + u^{\text{out}} \tag{3}$$

and that the incoming wave $u^{\text{in}} = \mathrm{e}^{-\mathrm{i}kx}$. Substituting u from Eq. (3) in Eq. (2), as well as further simplifying yields

$$\nabla \cdot \left(\frac{1}{\epsilon}\nabla u^{\text{out}}\right) + k^2 u^{\text{out}} = -\left(\frac{1}{\epsilon} - 1\right)\nabla \cdot \nabla u^{\text{in}}. \tag{4}$$

Consider the problem setup illustrated in Fig. 1, where Ω^{D} is the design domain that is surrounded by Ω^{air}. The size of Ω^{D} is 100 nm $\times$ 100 nm. It is surrounded by Ω^{air} of thickness 60 nm on all four sides. In this setup, we study the average temperature in Ω^{T}. The size of Ω^{T} is 10 nm $\times$ 10 nm. Moreover, we introduce a PML region Ω^{PML} of thickness $d = 40$ nm that approximates the far-field condition, where ($x^{\min}$, $y^{\min}$) and ($x^{\max}$, $y^{\max}$) are the coordinates of the computational domain Ω's outer bounds.

With a TE-polarized incoming wave, we study the temperature in Ω^{T} when parts of Ω^{D} are occupied by silver and the rest of $\mathbb{R}^2$ is occupied by air. The

permittivity of silver has a negative real part and exhibits strong dielectric characteristics at plasmonic wavelengths. We study the case where the wavelength of the incoming wave is 413 nm. At this wavelength, the permittivity values of silver and air are $\epsilon_{\text{Ag}} = -5.0012 + 0.1295\text{i}$ [22] and $\epsilon_{\text{air}} = 1$, respectively.

The variational form of Eq. (4) with a PML for the outgoing wave u^{out} is presented below.

Find $u^{\text{out}} \in H^1(\Omega)$, such that:

$$k^2 \int_\Omega \zeta u^{\text{out}} v - \int_\Omega (\boldsymbol{D}\nabla u^{\text{out}}) \cdot \nabla v - \int_{\Omega^{\text{D}}} \left(\frac{1}{\epsilon} - 1\right) \nabla u^{\text{out}} \cdot \nabla v = -\int_{\Omega^{\text{D}}} \left(\frac{1}{\epsilon} - 1\right) \nabla u^{\text{in}} \cdot \nabla v, \quad v \in H^1(\Omega). \tag{5}$$

The diagonal matrix $\boldsymbol{D} = \text{diag}(\alpha_y/\alpha_x, \alpha_x/\alpha_y)$ and $\zeta = \alpha_x \alpha_y$, where

$$\begin{aligned} \alpha_x &= 1 + \text{i}\sigma_0 \sigma_x, \\ \alpha_y &= 1 + \text{i}\sigma_0 \sigma_y, \end{aligned} \tag{6}$$

in which σ_0 is a positive constant and

$$\begin{aligned} \sigma_x &= \max(0, \max(x - x^{\max} + d, x^{\min} + d - x)), \\ \sigma_y &= \max(0, \max(y - y^{\max} + d, y^{\min} + d - y)). \end{aligned} \tag{7}$$

Moreover, we let

$$\eta(x) = \frac{1}{\epsilon(x)} - 1, \quad \text{so} \quad \epsilon(x) = \frac{1}{\eta(x) + 1}. \tag{8}$$

Putting η in Eq. (5) yields the problem below.

Find $u^{\text{out}} \in H^1(\Omega)$, such that

$$k^2 \int_\Omega \zeta u^{\text{out}} v - \int_\Omega (\boldsymbol{D}\nabla u^{\text{out}}) \cdot \nabla v - \int_{\Omega^{\text{D}}} \eta \nabla u^{\text{out}} \cdot \nabla v = -\int_{\Omega^{\text{D}}} \eta \nabla u^{\text{in}} \cdot \nabla v, \quad v \in H^1(\Omega). \tag{9}$$

The variational form above computes the outgoing wave u^{out} of the total field u. To compute the temperature field in the computational domain, Helmholtz equation (4) is coupled to a Poisson equation of the form

$$-\nabla \cdot \kappa \nabla T = \text{Im}(\epsilon) u \bar{u}, \quad \text{in} \quad \Omega, \tag{10}$$

$$T = T_\infty, \qquad \text{on} \quad \Gamma^{\text{D}}, \tag{11}$$

where κ is the thermal conductivity, T_∞ is the ambient temperature, and the imaginary part of ϵ times the square amplitude of total field u enter as a forcing to the Poisson problem. Without loss of generality, we set $T_\infty = 0$, so the solution $\boldsymbol{T}$ is the temperature difference with respect to the true ambient temperature.

The variational form of Poisson problem (10) with boundary condition (11) is

$$\begin{aligned} &\text{Find } v \in \mathcal{V}, \text{ such that:} \\ &\int_\Omega \kappa \nabla T \cdot \nabla q = \int_\Omega \operatorname{Im}\left(\frac{1}{\eta + 1}\right) u \bar{u}\, q, \quad q \in \mathcal{V}, \end{aligned} \tag{12}$$

where $\mathcal{V} = \{v \in H^1(\Omega) \big| \, v|_{\Gamma^{\mathrm{D}}} \equiv 0\}$.

The objective function that measures the integrated temperature over Ω^{T} is

$$J = \int_{\Omega^{\mathrm{T}}} T. \tag{13}$$

Remark. This coupled plasmonic problem is selected to capture important issues concerning non-linearly coupled complex–real field problems.

We want to perform the sensitivity analysis on this problem using the adjoint method. More precisely, we want to compute gradients of the objective function with respect to η and κ. Performing sensitivity analysis of the coupled plasmonic problem presents several challenging issues, as it involves the coupling of the complex field u with Poisson equation (10). To address these issues, we first examine a model problem that has many of the same characteristics as the plasmonic problem but avoids the issues stemming from the complex solution of the plasmonic problem. Nevertheless, it aids in a better understanding of the main problem.

3 A model problem

We investigate a simple model problem, in which a Poisson equation is coupled to another Poisson equation defined on the domain Ω, which is illustrated in Fig. 2. The first Poisson equation with boundary conditions is expressed as

$$-\nabla \cdot \eta \nabla u = 1, \quad \text{in} \quad \Omega, \tag{14}$$

$$u = 0, \quad \text{on} \quad \Gamma^{\mathrm{D}}, \tag{15}$$

$$n \cdot \nabla u = 0, \quad \text{on} \quad \Gamma^{\mathrm{N}}. \tag{16}$$

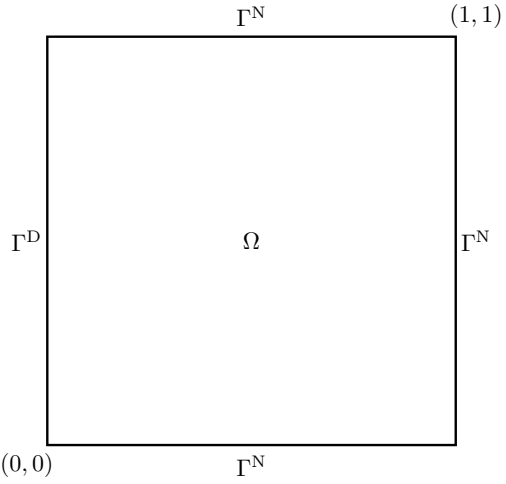

Figure 2: Computational domain Ω for the model problem

The real-valued field u of first Poisson equation (14) is nonlinearly coupled to a second Poisson equation as

$$-\nabla \cdot \kappa \nabla T = \eta\, u^2, \quad \text{in} \quad \Omega, \tag{17}$$

$$T = 0, \quad \text{on} \quad \Gamma^{\mathrm{D}}, \tag{18}$$

$$n \cdot \nabla T = 0, \quad \text{on} \quad \Gamma^{\mathrm{N}}. \tag{19}$$

To derive variational forms, we multiply Eqs. (14) and (17) with test functions v and q, respectively, and integrate by parts. Moreover, we define $\mathcal{V} = \{v \in H^1(\Omega) \big| \, v|_{\Gamma^{\mathrm{D}}} \equiv 0\}$.

The variational form of first Poisson Eq. (14) with boundary conditions (15)–(16) reads

$$\begin{gathered} \text{Find } u \in \mathcal{V} \text{ with such that:} \\ \int_\Omega \eta \nabla u \cdot \nabla v = \int_\Omega v \quad \forall\, v \in \mathcal{V}. \end{gathered} \tag{20}$$

Similarly, the variational form of second Poisson Eq. (17) with boundary conditions (18)–(19) reads

$$\begin{gathered} \text{Find } T \in \mathcal{V} \text{ such that:} \\ \int_\Omega \kappa \nabla T \cdot \nabla q = \int_\Omega \eta\, u^2 q \quad \forall\, q \in \mathcal{V}. \end{gathered} \tag{21}$$

The objective function, in this case, is an integral of T over the full domain Ω. That is,

$$J = \int_\Omega T. \tag{22}$$

3.1 Sensitivity analysis

Below, we derive expressions for the gradient of J with respect to η and κ for our model problem.

3.1.1 Gradient of the objective function with respect to η

Consider a design perturbation $\delta\eta$. We denote the induced first-order perturbation of J, u, and T by δJ, δu, and δT, respectively. The first-order perturbation of objective function (22) is

$$\delta J = \int_\Omega \delta T. \tag{23}$$

In addition, the perturbation of variational forms (20) and (21) reads

$$\int_\Omega \delta\eta \, \nabla u \cdot \nabla v + \int_\Omega \eta \, \nabla \delta u \cdot \nabla v = 0, \quad \forall \, v \in \mathcal{V} \tag{24}$$

and

$$\int_\Omega \kappa \, \nabla \delta T \cdot \nabla q = \int_\Omega \delta\eta \, u^2 \, q + 2 \int_\Omega \eta \, u \delta u \, q, \quad \forall \, q \in \mathcal{V}, \tag{25}$$

respectively.

First, we pick $z^{(1)}$ as the solution to the first adjoint problem

$$\begin{aligned} &\text{Find } z^{(1)} \in \mathcal{V}, \text{ such that} \\ &\int_\Omega \kappa \, \nabla v \cdot \nabla z^{(1)} = \int_\Omega v, \quad \forall \, v \in \mathcal{V}. \end{aligned} \tag{26}$$

Eq. (25) holds $\forall \, q$, so in particular it holds for $z^{(1)}$. Hence

$$\int_\Omega \kappa \nabla \delta T \cdot \nabla z^{(1)} = \int_\Omega \delta\eta \, u^2 \, z^{(1)} + 2 \int_\Omega \eta \, u \delta u \, z^{(1)}. \tag{27}$$

Since $z^{(1)}$ solves Eq. (26), we know that the left hand side of the above equation equals δJ, so

$$\delta J = \int_\Omega \delta\eta \, u^2 \, z^{(1)} + 2 \int_\Omega \eta \, u \delta u \, z^{(1)}. \tag{28}$$

To deal with the last integral term in expression (28), we pick $z^{(2)}$ as the solution to the second adjoint problem

$$\begin{aligned} &\text{Find } z^{(2)} \in \mathcal{V}, \text{ such that} \\ &\int_\Omega \eta \, \nabla q \cdot \nabla z^{(2)} = 2 \int_\Omega \eta \, u \, z^{(1)} \, q, \quad \forall \, q \in \mathcal{V}. \end{aligned} \tag{29}$$

Since expression (29) holds $\forall \, q$, we can choose $q = \delta u$. Thus

$$\int_\Omega \eta \, \nabla \delta u \cdot \nabla z^{(2)} = 2 \int_\Omega \eta \, u \, z^{(1)} \delta u. \tag{30}$$

Setting $v = z^{(2)}$ in Eq. (24) yields

$$\int_\Omega \delta\eta \, \nabla u \cdot \nabla z^{(2)} + \int_\Omega \eta \, \nabla \delta u \cdot \nabla z^{(2)} = 0. \tag{31}$$

Combining Eq. (30) and Eq. (31), we conclude that

$$2 \int_\Omega \eta \, u \, z^{(1)} \, \delta u = - \int_\Omega \delta\eta \, \nabla u \cdot \nabla z^{(2)}. \tag{32}$$

The left hand side above equals the last term in expression (28). Hence,

$$\delta J = \int_\Omega \delta\eta \, u^2 \, z^{(1)} - \int_\Omega \delta\eta \, \nabla u \cdot \nabla z^{(2)}. \tag{33}$$

3.1.2 Gradient of the objective function with respect to κ

For the Poisson equation, the gradients of J with respect to κ are standard and well known. Therefore, without going into details, we simply state that given a design perturbation $\delta\kappa$, the corresponding first-order perturbation of J is

$$\delta J = - \int_\Omega \delta\kappa \, \nabla T \cdot \nabla z^{(1)}. \tag{34}$$

Here, we do not solve another adjoint equation, as the adjoint equation for this problem is equivalent to Eq. (26) for $z^{(1)}$. Hence, in total, we solve two adjoint equations to determine sensitivities with respect to perturbations of η and κ for the model problem.

3.2 Finite element discretization

3.2.1 The variational forms

We triangulate Ω by using a uniform mesh of M square elements denoted Ω_m, $m = 1, 2, \ldots, M$. Let $\mathcal{V}_h$ be the space of functions that are bi-linear on each element and zero on Γ^{D}. The function u and the test function v are approximated by $u_h \in \mathcal{V}_h$ and $v_h \in \mathcal{V}_h$, respectively. Moreover, η is approximated by an element-wise constant function η_h. The discretized version of variational form (20) reads

$$\begin{aligned} &\text{Find } u_h \in \mathcal{V}_h \text{ such that} \\ &\int_\Omega \eta_h \nabla u_h \cdot \nabla v_h = \int_\Omega v_h, \quad \forall\, v_h \in \mathcal{V}_h. \end{aligned} \tag{35}$$

To compute finite element approximation u_h, we let $\{\varphi_i\}_{i=1}^n$ be the standard bi-linear nodal basis of $\mathcal{V}_h$ where n is the number of nodes in finite element approximation. The above equation can be written in matrix form as

$$\boldsymbol{K}\big[\boldsymbol{\eta}\big]\boldsymbol{u} = \boldsymbol{f}, \tag{36}$$

where $\boldsymbol{u}$ is the $n \times 1$ vector of unknowns, the $M \times 1$ vector $\boldsymbol{\eta}$ holds element values of η_h, the $n \times n$ matrix $\boldsymbol{K}\big[\boldsymbol{\eta}\big]$, and the $n \times 1$ vector $\boldsymbol{f}$ have entries

$$K_{ij} = \int_\Omega \eta_h \nabla \varphi_i \cdot \nabla \varphi_j \quad \text{and} \quad f_i = \int_\Omega \varphi_i, \tag{37}$$

respectively.

The function T and the test function q are approximated by $T_h \in \mathcal{V}_h$ and $q_h \in \mathcal{V}_h$, respectively. In addition, κ, like η, is approximated by an element-wise function κ_h. The discretized version of second variational form (21) reads

$$\begin{aligned} &\text{Find } T_h \in \mathcal{V}_h \text{ such that} \\ &\int_\Omega \kappa_h \nabla T_h \cdot \nabla q_h = \int_\Omega \eta_h\, u_h^2\, q_h \quad \forall\, q_h \in \mathcal{V}_h. \end{aligned} \tag{38}$$

Similarly, to compute finite element approximation T_h, we again use $\{\varphi_i\}_{i=1}^n$ as a basis of $\mathcal{V}_h$. In Eq. (38), the function u_h^2 is not bi-linear and thus, does not belong to $\mathcal{V}_h$. To approximate u_h^2, we use its nodal interpolants. Therefore, the above equation can be approximated in matrix form as

$$\boldsymbol{A}\big[\boldsymbol{\kappa}\big]\boldsymbol{T} = \boldsymbol{M}\big[\boldsymbol{\eta}\big]\,(\boldsymbol{u} \odot \boldsymbol{u}), \tag{39}$$

where the $M \times 1$ vector $\boldsymbol{\kappa}$ holds element values of κ_h, $\boldsymbol{T}$ is the $n \times 1$ vector of unknowns, and the operator $\odot$ represents elementwise multiplication of two

vectors. Moreover, the $n \times n$ matrix $\boldsymbol{A}\big[\boldsymbol{\kappa}\big]$ and the $n \times n$ matrix $\boldsymbol{M}\big[\boldsymbol{\eta}\big]$ have entries

$$A_{ij} = \int_{\Omega} \kappa_h \nabla\varphi_i \cdot \nabla\varphi_j \quad \text{and} \quad M_{ij} = \int_{\Omega} \eta_h \, \varphi_i \, \varphi_j, \tag{40}$$

respectively.

Remark. An alternative way to evaluate the right hand side of Eq. (38) is to use quadrature. More precisely, Eq. (38) can be written in matrix form as

$$\boldsymbol{A}\big[\boldsymbol{\kappa}\big]\boldsymbol{T} = \boldsymbol{b}\big[\boldsymbol{\eta}\big], \tag{41}$$

where the entries of $n \times 1$ vector $\boldsymbol{b}\big[\boldsymbol{\eta}\big]$

$$b_i = \int_{\Omega} \eta_h \, u_h^2 \varphi_i, \tag{42}$$

are evaluated using the quadrature. Using both of the aforementioned approaches, numerical experiments were carried out to compute the T-field distribution in Ω with varying mesh resolutions. The maximum difference between the solutions is $O(h^2)$, which is the same order as the error of the finite element solution. Hence, we use nodal interpolants to approximate the function, as this is computationally less expensive than quadrature.

3.2.2 Gradients

Having solved Eqs. (36) and (39) for $\boldsymbol{u}$ and $\boldsymbol{T}$, respectively, the sensitivities of J with respect to a perturbation $\delta\boldsymbol{\eta}$ of $\boldsymbol{\eta}$ are

$$\delta J = \big(\boldsymbol{u} \odot \boldsymbol{u}\big)^T \boldsymbol{M}\big[\delta\boldsymbol{\eta}\big] \, \boldsymbol{z}^{(1)} - \boldsymbol{u}^T \boldsymbol{K}\big[\delta\boldsymbol{\eta}\big] \, \boldsymbol{z}^{(2)}, \tag{43}$$

where the $n \times 1$ vectors $\boldsymbol{z}^{(1)}$ and $\boldsymbol{z}^{(2)}$ solve the following two adjoint equations

$$\boldsymbol{A}\big[\boldsymbol{\kappa}\big]\boldsymbol{z}^{(1)} = \boldsymbol{f}, \tag{44}$$

and

$$\boldsymbol{K}\big[\boldsymbol{\eta}\big]\boldsymbol{z}^{(2)} = 2\left(\boldsymbol{M}\big[\boldsymbol{\eta}\big] \, \boldsymbol{z}^{(1)}\right) \odot \boldsymbol{u}, \tag{45}$$

respectively.

Using expression (43), we identify gradients of J with respect to η_m, the mth entry in $\boldsymbol{\eta}$, as

$$\frac{\partial J}{\partial \eta_m} = \big(\boldsymbol{u} \odot \boldsymbol{u}\big)^T \boldsymbol{M}_m \, \boldsymbol{z}^{(1)} - \boldsymbol{u}^T \boldsymbol{K}_m \, \boldsymbol{z}^{(2)}, \quad m = 1, 2, \ldots, M, \tag{46}$$

where the $n \times n$ element mass matrix $\boldsymbol{M}_m$ and the $n \times n$ element stiffness matrix $\boldsymbol{K}_m$ have entries

$$M_m = \int_{\Omega_m} \varphi_i \, \varphi_j \quad \text{and} \quad K_m = \int_{\Omega_m} \nabla \varphi_i \cdot \nabla \varphi_j, \tag{47}$$

respectively.

Similarly to Eq. (46), we identify the gradients of J with respect to κ_m, the mth entry of $\boldsymbol{\kappa}$, using Eq. (34)

$$\frac{\partial J}{\partial \kappa_m} = -\boldsymbol{T}^T \boldsymbol{A}_m \, \boldsymbol{z}^{(1)}, \quad m = 1, 2, \ldots, M. \tag{48}$$

Remark. The mass $\boldsymbol{M}_m$ and the stiffness matrices $\boldsymbol{K}_m$ and $\boldsymbol{A}_m$ only have non-zero entries on the nodal values corresponding to the element Ω_m. As we have a uniform mesh, we instead use the element mass $\boldsymbol{M}^{\mathrm{EL}}$ and stiffness $\boldsymbol{K}^{\mathrm{EL}}$ and $\boldsymbol{A}^{\mathrm{EL}}$ matrices of size 4×4. Moreover, we use subvectors $\boldsymbol{u}_m$, $\boldsymbol{z}_m^{(1)}$, and $\boldsymbol{z}_m^{(2)}$, which hold nodal values in Ω_m of $\boldsymbol{u}$, $\boldsymbol{z}^{(1)}$, and $\boldsymbol{z}^{(2)}$, respectively. More precisely, we evaluate the following two expressions to compute the mth entry of sensitivities with respect to perturbed η and κ

$$\frac{\partial J}{\partial \eta_m} = \left(\boldsymbol{u}_m \odot \boldsymbol{u}_m\right)^T \boldsymbol{M}^{\mathrm{EL}} \, \boldsymbol{z}_m^{(1)} - \boldsymbol{u}_m^T \, \boldsymbol{K}^{\mathrm{EL}} \, \boldsymbol{z}_m^{(2)}, \quad m = 1, 2, \ldots, M, \tag{49}$$

and

$$\frac{\partial J}{\partial \kappa_m} = -\boldsymbol{T}_m^T \boldsymbol{A}^{\mathrm{EL}} \, \boldsymbol{z}_m^{(1)}, \quad m = 1, 2, \ldots, M, \tag{50}$$

respectively.

3.3 Results for the model problem

We use a minimal example to validate gradients by dividing Ω into four elements with a side length $\Delta x = 0.5$. We choose a coarse mesh for the computational domain so that we can validate the gradients of the objective function with respect to all four elements using the finite difference approach. For the Poisson equation, the gradients of the objective function with respect to κ are well known. Hence, we only show results for the gradients with respect to η for validation. The matrix form of objective function (13) reads

$$J\left(\boldsymbol{\kappa}, \boldsymbol{\eta}\right) = \boldsymbol{g}_1^T \boldsymbol{T}, \tag{51}$$

where $\boldsymbol{g}_1$ is a $n \times 1$ vector of ones.

The objective function $J = 2.5836$ with randomly selected $\boldsymbol{\kappa} = (0.8003, 0.1419, 0.4218, 0.9157)^T$ and $\boldsymbol{\eta} = (0.1576, 0.9706, 0.9572, 0.4854)^T$. Moreover, with the adjoint method, the range of gradients with respect to η is $[-5.8736, 1.2471]$. To validate our sensitivity analysis in Eq. (46), we use a forward first-order finite difference scheme

$$\frac{\partial J}{\partial \eta_m} \approx \frac{J\big(\boldsymbol{\kappa}, \boldsymbol{\eta} + h\boldsymbol{e}_m\big) - J\big(\boldsymbol{\kappa}, \boldsymbol{\eta}\big)}{h}, \quad m = 1, \ldots, M, \tag{52}$$

where h is the finite difference step size and $\boldsymbol{e}_m$ is the mth unit vector.

We employ an absolute difference scaled by the maximum value to compare the sensitivities computed using the adjoint and the finite difference approach. More precisely, we use the following expression

$$\text{Relative Absolute Difference} = \frac{|x_m - y_m|}{\max_n |x_n|}, \quad m, n = 1, 2, \ldots, M, \tag{53}$$

where x_m and y_m represent $\partial J/\partial \eta_m$ evaluated using the adjoint and the finite difference approach, respectively. In addition, the scaling value in the denominator is the maximum absolute value of gradients by the adjoint method. Fig. 3 illustrates that the relative absolute difference between gradients computed using the adjoint and finite difference methods converges linearly. We also performed an additional numerical experiment with a fine mesh of 10,000 elements in Ω. The results of this experiment follow the same trend, as seen in Fig. 3.

4 The coupled plasmonic problem

After examining the test problem and verifying the sensitivity analysis with the finite difference method, we move on to the main problem presented in Section 2.

4.1 Sensitivity analysis

4.1.1 Gradient of objective function with respect to η

Consider a design perturbation $\delta\eta$ and denote the induced first-order perturbation of J, u^{out}, and T by δJ, δu^{out}, and δT, respectively. The first-order perturbations of objective function (13), and variation forms (9) and (12) read as follows:

$$\delta J = \int_{\Omega^{\text{T}}} \delta T, \tag{54}$$

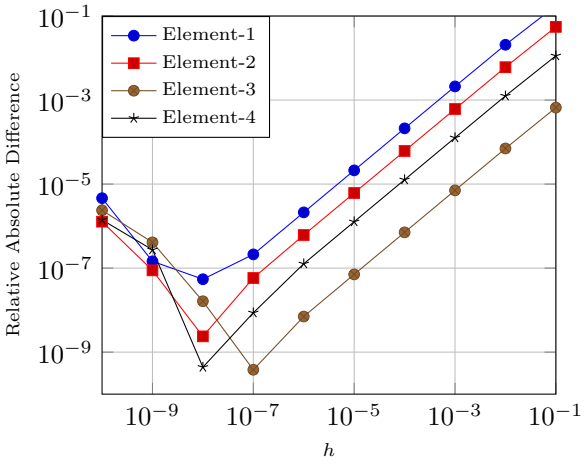

Figure 3: The relative absolute difference in gradients of the objective function with respect to η for the model problem, computed using the adjoint and the finite difference method, is plotted against the finite difference h for all four elements in the computational domain Ω.

$$k^2 \int_\Omega \zeta \delta u^{\text{out}} v \; - \int_\Omega (\boldsymbol{D} \nabla \delta u^{\text{out}}) \cdot \nabla v \; - \int_{\Omega^{\text{D}}} \eta \nabla \delta u^{\text{out}} \cdot \nabla v$$
$$= \int_{\Omega^{\text{D}}} \delta\eta \nabla u^{\text{out}} \cdot \nabla v - \int_{\Omega^{\text{D}}} \delta\eta \nabla u^{\text{in}} \cdot \nabla v, \quad v \in \mathcal{V}, \quad (55)$$

and

$$\int_\Omega \kappa \, \nabla \delta T \cdot \nabla q = \int_{\Omega^{\text{D}}} \delta \, \text{Im}\left(\frac{1}{\eta + 1}\right) u \bar{u} \, q$$
$$+ \int_{\Omega^{\text{D}}} \text{Im}\left(\frac{1}{\eta + 1}\right) \left(\delta u^{\text{out}} \, \bar{u} + u \, \delta \bar{u}^{\text{out}}\right) q \quad \forall \, q \in \mathcal{V}, \quad (56)$$

respectively. Note that we have reordered the terms in Eq. (55) by moving $\delta\eta$ terms to the right hand side.

We select $z^{(1)}$ as the solution to the first adjoint problem

$$\begin{aligned} &\text{Find } z^{(1)} \in \mathcal{V} \text{ such that} \\ &\int_\Omega \kappa \, \nabla v \cdot \nabla z^{(1)} = \int_{\Omega^{\text{T}}} v, \quad \forall \, v \in \mathcal{V}. \end{aligned} \quad (57)$$

Eq. (56) holds $\forall v$, which means it in particular holds for $z^{(1)}$. So,

$$\int_\Omega \kappa \nabla \delta T \cdot \nabla z^{(1)} = \int_{\Omega^{\mathrm{D}}} \delta \operatorname{Im}\left(\frac{1}{\eta+1}\right) u\bar{u}\, z^{(1)} + \int_{\Omega^{\mathrm{D}}} \operatorname{Im}\left(\frac{1}{\eta+1}\right) \left(\delta u^{\mathrm{out}}\, \bar{u} + u\, \delta \bar{u}^{\mathrm{out}}\right) z^{(1)}. \quad (58)$$

Since $z^{(1)}$ solves adjoint Eq. (57), we have the left hand side of the above equation equals $\int_{\Omega^{\mathrm{T}}} \delta T = \delta J$, thus

$$\delta J = \int_{\Omega^{\mathrm{D}}} \delta \operatorname{Im}\left(\frac{1}{\eta+1}\right) u\bar{u}\, z^{(1)} + \int_{\Omega^{\mathrm{D}}} \operatorname{Im}\left(\frac{1}{\eta+1}\right) \left(\delta u^{\mathrm{out}}\, \bar{u} + u\, \delta \bar{u}^{\mathrm{out}}\right) z^{(1)}. \quad (59)$$

Remark. It might be tempting to deal with the last integral term in expression (59) similarly, as we dealt with the coupled Poisson–Poisson case. However, in general, there is no $z^{(2)}$ that satisfies the following equation

$$k^2 \int_\Omega \zeta\, q\, z^{(2)} - \int_\Omega (\boldsymbol{D} \nabla q) \cdot \nabla z^{(2)} - \int_{\Omega^{\mathrm{D}}} \eta \nabla q \cdot \nabla z^{(2)} = \int_{\Omega^{\mathrm{D}}} \operatorname{Im}\left(\frac{1}{\eta+1}\right) \left(q\, \bar{u} + u\, \bar{q}\right) z^{(1)}, \quad \forall\, q \in \mathcal{V}. \quad (60)$$

(Note if for example, $\operatorname{Im}(\eta) = 0$, $u = 0$, or $z^{(1)} = 0$, then $z^{(2)}$ trivially solves the problem.)

A key difference is that, for the model problem u is a real-valued field while for the plasmonic problem u^{out} is a complex field. In general, to obtain sensitivities we need two additional adjoints equations.

First, we deal with δu^{out} in Eq. (59) by selecting $z^{(2)}$ as the solution to the second ajoint problem

Find $z^{(2)} \in \mathcal{V}$ such that

$$k^2 \int_\Omega \zeta\, q\, z^{(2)} - \int_\Omega (\boldsymbol{D} \nabla q) \cdot \nabla z^{(2)} - \int_{\Omega^{\mathrm{D}}} \eta \nabla q \cdot \nabla z^{(2)} = \int_{\Omega^{\mathrm{D}}} \operatorname{Im}\left(\frac{1}{\eta+1}\right) q\, \bar{u}\, z^{(1)}, \quad \forall\, q \in \mathcal{V}. \quad (61)$$

Since expression (61) holds $\forall\, q$, we can choose $q = \delta u^{\mathrm{out}}$. Hence

$$k^2 \int_\Omega \zeta\, \delta u^{\mathrm{out}} z^{(2)} - \int_\Omega (\boldsymbol{D} \nabla \delta u^{\mathrm{out}}) \cdot \nabla z^{(2)} - \int_{\Omega^{\mathrm{D}}} \eta \nabla \delta u^{\mathrm{out}} \cdot \nabla z^{(2)} = \int_{\Omega^{\mathrm{D}}} \operatorname{Im}\left(\frac{1}{\eta+1}\right) \delta u^{\mathrm{out}}\, \bar{u} z^{(1)}. \quad (62)$$

The left hand side of the above expression is identical to the left hand side of expression (55) for the particular choice $v = z^{(2)}$. Thus

$$\int_{\Omega^{\mathrm{D}}} \mathrm{Im}\left(\frac{1}{\eta+1}\right) \delta u^{\mathrm{out}}\, \bar{u}\, z^{(1)} = \int_{\Omega^{\mathrm{D}}} \delta\eta \nabla u^{\mathrm{out}} \cdot \nabla z^{(2)} - \int_{\Omega^{\mathrm{D}}} \delta\eta \nabla u^{\mathrm{in}} \cdot \nabla z^{(2)}. \tag{63}$$

Similarly, we deal with $\delta\bar{u}^{\mathrm{out}}$ in Eq. (59) by selecting $z^{(3)}$ as the solution to the third adjoint problem

Find $z^{(3)} \in \mathcal{V}$ such that

$$k^2 \int_{\Omega} \bar{\zeta}\, p\, z^{(3)} - \int_{\Omega} (\overline{\boldsymbol{D}} \nabla p) \cdot \nabla z^{(3)} - \int_{\Omega^{\mathrm{D}}} \bar{\eta} \nabla p \cdot \nabla z^{(3)} = \int_{\Omega^{\mathrm{D}}} \mathrm{Im}\left(\frac{1}{\eta+1}\right) p\, u\, z^{(1)}, \quad \forall\, p \in \mathcal{V}. \tag{64}$$

Again, as expression (64) holds $\forall\, p$, it in particular holds for $\delta\bar{u}^{\mathrm{out}}$; so

$$k^2 \int_{\Omega} \bar{\zeta}\, \delta\bar{u}^{\mathrm{out}} z^{(3)} - \int_{\Omega} (\overline{\boldsymbol{D}} \nabla \delta\bar{u}^{\mathrm{out}}) \cdot \nabla z^{(3)} - \int_{\Omega^{\mathrm{D}}} \bar{\eta} \nabla \delta\bar{u}^{\mathrm{out}} \cdot \nabla z^{(3)} = \int_{\Omega^{\mathrm{D}}} \mathrm{Im}\left(\frac{1}{\eta+1}\right) \delta\bar{u}^{\mathrm{out}}\, u z^{(1)}. \tag{65}$$

The left hand side of the above expression is identical to the conjugate of left hand side of expression (55) for the particular choice $v = z^{(3)}$, which entails

$$\int_{\Omega^{\mathrm{D}}} \mathrm{Im}\left(\frac{1}{\eta+1}\right) \delta\bar{u}^{\mathrm{out}}\, u\, z^{(1)} = \int_{\Omega^{\mathrm{D}}} \delta\bar{\eta} \nabla \bar{u}^{\mathrm{out}} \cdot \nabla z^{(3)} - \int_{\Omega^{\mathrm{D}}} \delta\bar{\eta} \nabla \bar{u}^{\mathrm{in}} \cdot \nabla z^{(3)}. \tag{66}$$

The sum of the left hand sides of expressions (63) and (66) equals the last term in expression (59). Thus

$$\delta J = \int_{\Omega^{\mathrm{D}}} \delta\, \mathrm{Im}\left(\frac{1}{\eta+1}\right) u\bar{u}\, z^{(1)} + \int_{\Omega^{\mathrm{D}}} \delta\eta \nabla (u^{\mathrm{out}} - u^{\mathrm{in}}) \cdot \nabla z^{(2)} + \int_{\Omega^{\mathrm{D}}} \delta\bar{\eta} \nabla (\bar{u}^{\mathrm{out}} - \bar{u}^{\mathrm{in}}) \cdot \nabla z^{(3)}. \tag{67}$$

Remark. In this case, $z^{(1)}$ is real and hence, $z^{(2)} = \bar{z}^{(3)}$. Moreover, the last term in Eq. (67) is a conjugate of the second term. Therefore, we do not need to compute $z^{(3)}$. Moreover, expression (67) reduces to

$$\delta J = \int_{\Omega^{\mathrm{D}}} \delta \operatorname{Im}\left(\frac{1}{\eta+1}\right) u\bar{u}\, z^{(1)} + 2\int_{\Omega^{\mathrm{D}}} \operatorname{Re}\big\{\delta\eta\nabla\big(u^{\mathrm{out}} - u^{\mathrm{in}}\big)\cdot\nabla z^{(2)}\big\}. \quad (68)$$

For the plasmonic problem, the gradients of objective function (13) with respect to κ are similar to the model problem presented in Section 3.1.2. Thus, also in this case, it is sufficient to solve two adjoint equations to determine the sensitivities with respect to η and κ.

4.2 Finite element discretization

4.2.1 The variational forms

The variational form (9) of TE-polarized Helmholtz equation can be written in matrix form as

$$\Big(k^2\boldsymbol{M} - \boldsymbol{K} - \boldsymbol{B}\big[\boldsymbol{\eta}\big]\Big)\boldsymbol{u}^{\mathrm{out}} = \boldsymbol{B}\big[\boldsymbol{\eta}\big]\boldsymbol{u}^{\mathrm{in}}, \quad (69)$$

where $\boldsymbol{u}^{\mathrm{out}}$ is the $n\times 1$ vector of unknowns and $\boldsymbol{u}^{\mathrm{in}}$ is the $n\times 1$ vector of nodal values of u^{in}, and the $n\times n$ matrix $\boldsymbol{M}$, the $n\times n$ matrix $\boldsymbol{K}$, and the $n\times n$ matrix $\boldsymbol{B}\big[\boldsymbol{\eta}\big]$ have entries

$$M_{ij} = \int_\Omega \zeta\varphi_i\,\varphi_j, \quad K_{ij} = \int_\Omega (\boldsymbol{D}\nabla\varphi_i)\cdot\nabla\varphi_j, \quad \text{and} \quad B_{ij} = \int_\Omega \eta_h\nabla\varphi_i\cdot\nabla\varphi_j, \quad (70)$$

respectively.

Similarly, the variational form (12) of Poisson equation can be approximated in matrix form as

$$\boldsymbol{A}(\boldsymbol{\kappa})\boldsymbol{T} = \boldsymbol{M}\left[\operatorname{Im}\left(\frac{1}{\boldsymbol{\eta}+1}\right)\right](\boldsymbol{u}\odot\overline{\boldsymbol{u}}), \quad (71)$$

where $\boldsymbol{T}$ is the $n\times 1$ vector of unknowns, and the $n\times n$ matrix $\boldsymbol{A}\big[\boldsymbol{\kappa}\big]$, and the $n\times n$ matrix $\boldsymbol{M}\left[\operatorname{Im}\left(\frac{1}{\eta_h+1}\right)\right]$ have entries

$$A_{ij} = \int_\Omega \kappa_h\nabla\varphi_i\cdot\nabla\varphi_j, \quad \text{and} \quad M_{ij} = \int_\Omega \operatorname{Im}\left(\frac{1}{\eta_h+1}\right)\varphi_i\,\varphi_j, \quad (72)$$

respectively.

4.2.2 Gradients

The sensitivities of J with respect to perturbed $\boldsymbol{\eta}$ can be written as

$$\delta J = \big(\boldsymbol{u} \odot \overline{\boldsymbol{u}}\big)^T \boldsymbol{M} \left[\delta \mathrm{Im}\left(\frac{1}{\boldsymbol{\eta}+1}\right)\right] \boldsymbol{z}_1 + \boldsymbol{u}^T \boldsymbol{B}\big[\delta\boldsymbol{\eta}\big]\, \boldsymbol{z}^{(2)} + \overline{\boldsymbol{u}}^T \boldsymbol{B}\big[\delta\boldsymbol{\eta}\big]\, \overline{\boldsymbol{z}}^{(2)}, \quad (73)$$

where $n \times 1$ vectors $\boldsymbol{z}^{(1)}$ and $\boldsymbol{z}^{(2)}$ solve the two adjoint equations

$$\boldsymbol{A}\big[\boldsymbol{\kappa}\big]\boldsymbol{z}^{(1)} = \boldsymbol{f}, \quad (74)$$

in which the $n \times 1$ vector $\boldsymbol{f}$ has entries

$$f_i = \int_{\Omega^{\mathrm{T}}} \varphi_i, \quad (75)$$

and

$$\Big(k^2\boldsymbol{M} - \boldsymbol{K} - \boldsymbol{B}\big[\boldsymbol{\eta}\big]\Big)\boldsymbol{z}^{(2)} = \Big(\boldsymbol{M}\left[\mathrm{Im}\left(\frac{1}{\boldsymbol{\eta}+1}\right)\right]\boldsymbol{z}^{(1)}\Big) \odot \overline{\boldsymbol{u}}, \quad (76)$$

respectively.

Using expression (73), we identify gradients of J with respect to η_m, the mth element in $\boldsymbol{\eta}$, as

$$\frac{\partial J}{\partial \eta_m} = \big(\boldsymbol{u} \odot \overline{\boldsymbol{u}}\big)^T \boldsymbol{M}_m \left[\mathrm{Im}\left(\frac{-1}{\eta_m^2+1}\right)\right] \boldsymbol{z}^{(1)} + \boldsymbol{u}^T \boldsymbol{B}\, \boldsymbol{z}^{(2)} + \overline{\boldsymbol{u}}^T \boldsymbol{B}\, \overline{\boldsymbol{z}}^{(2)},$$
$$m = 1,\, 2,\, \ldots,\, M, \quad (77)$$

where the $n \times n$ element mass matrix $\boldsymbol{M}_m\left[\mathrm{Im}\left(\frac{-1}{\eta_m^2+1}\right)\right]$ and the $n \times n$ element stiffness matrix $\boldsymbol{B}_m$ have entries

$$M_m = \int_{\Omega_m} \mathrm{Im}\left(\frac{-1}{\eta_m^2+1}\right)\varphi_i\, \varphi_j \quad \text{and} \quad B_m = \int_{\Omega_m} \nabla\varphi_i \cdot \nabla\varphi_j, \quad (78)$$

respectively.

4.3 Results for the plasmonic problem

For the plasmonic problem, we use a fine mesh for the finite element discretization because the interface between the metal and air exhibits large amplitudes

of the electromagnetic field. Hence, we use $\Delta x = 0.5$ nm for the finite element discretization, which corresponds to 40,000 elements in Ω^{D} and 360,000 elements in Ω.

The objective function (13) in a matrix form is

$$J(\boldsymbol{\kappa}, \boldsymbol{\eta}) = \boldsymbol{g}_2^T \boldsymbol{T}, \tag{79}$$

where $\boldsymbol{g}_2$ is a $n \times 1$ vector of zeros and only contains ones at indices that correspond to nodes in Ω^{T}. Moreover, the value of J is 1.0299×10^{-12}.

To validate the sensitivity analysis of the coupled plasmonic problem presented in Eq. (77), we again use a forward first-order finite difference scheme presented in expressions (52). For the plasmonic problem, we cannot validate the gradients of all the 40,000 elements with the finite difference approach. Therefore, we randomly select ten elements to validate the sensitivity analysis with the finite difference method. The physical quantities in this problem are expressed in SI units. Therefore, the values of gradients are small due to nano scaling. More precisely, with the adjoint method, the range of gradients with respect to η is $[-7.2132 \times 10^{-15}, 6.1201 \times 10^{-16}]$. We again employ expression (53) to compute the relative absolute difference to validate our sensitivity analysis with the finite difference approach. Fig. 4 illustrates the placement of ten randomly selected elements for validation of gradients and the relative absolute difference between gradients computed using the adjoint method and the finite difference method converges linearly in h.

References

[1] Niels Aage, Erik Andreassen, Boyan S Lazarov, and Ole Sigmund. Giga-voxel computational morphogenesis for structural design. *Nature*, 550(7674):84–86, 2017.

[2] Niels Aage and V Egede Johansen. Topology optimization of microwave waveguide filters. *International Journal for Numerical Methods in Engineering*, 112(3):283–300, 2017.

[3] Niels Aage, NA Mortensen, and Ole Sigmund. Topology optimization of metallic devices for microwave applications. *International Journal for numerical methods in engineering*, 83(2):228–248, 2010.

[4] Moustafa RK Ali, Yue Wu, and Mostafa A El-Sayed. Gold-nanoparticle-assisted plasmonic photothermal therapy advances toward clinical application. *The Journal of Physical Chemistry C*, 123(25):15375–15393, 2019.

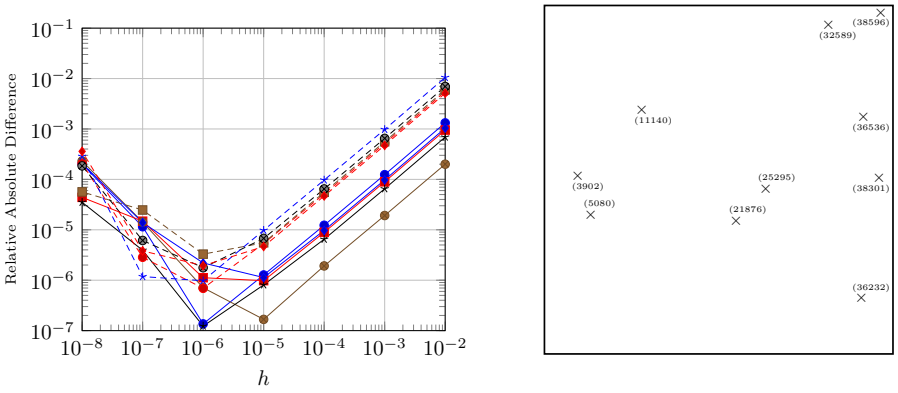

Figure 4: Left: The relative absolute difference in gradients of the objective function with respect to η for the plasmonic problem, computed using the adjoint and the finite difference method, is plotted against the finite difference h for randomly selected ten elements in the computational domain Ω. Right: Placement of randomly selected ten elements in Ω^{D} for the validation of gradients.

[5] Ahmad H Bokhari, Abbas Mousavi, Bin Niu, and Eddie Wadbro. Topology optimization of an acoustic diode? *Structural and Multidisciplinary Optimization*, 63(6):2739–2749, 2021.

[6] Thomas Borrvall and Joakim Petersson. Topology optimization of fluids in Stokes flow. *International journal for numerical methods in fluids*, 41(1):77–107, 2003.

[7] Alla B Bucharskaya, Galina N Maslyakova, Marina L Chekhonatskaya, Georgy S Terentyuk, Nikita A Navolokin, Boris N Khlebtsov, Nikolai G Khlebtsov, Alexey N Bashkatov, Elina A Genina, and Valery V Tuchin. Plasmonic photothermal therapy: Approaches to advanced strategy. *Lasers in surgery and medicine*, 50(10):1025–1033, 2018.

[8] Marco Cavazzuti, Andrea Baldini, Enrico Bertocchi, Dario Costi, Enrico Torricelli, and Patrizio Moruzzi. High performance automotive chassis design: a topology optimization based approach. *Structural and Multidisciplinary Optimization*, 44(1):45–56, 2011.

[9] Rasmus E Christiansen, Joakim Vester-Petersen, Søren Peder Madsen, and Ole Sigmund. A non-linear material interpolation for design of metallic

nano-particles using topology optimization. *Computer Methods in Applied Mechanics and Engineering*, 343:23–39, 2019.

[10] Maria B Dühring, Jakob S Jensen, and Ole Sigmund. Acoustic design by topology optimization. *Journal of sound and vibration*, 317(3-5):557–575, 2008.

[11] Emadeldeen Hassan, Daniel Noreland, Robin Augustine, Eddie Wadbro, and Martin Berggren. Topology optimization of planar antennas for wide-band near-field coupling. *IEEE Transactions on Antennas and Propagation*, 63(9):4208–4213, 2015.

[12] Emadeldeen Hassan, Eddie Wadbro, and Martin Berggren. Topology optimization of metallic antennas. *IEEE transactions on antennas and propagation*, 62(5):2488–2500, 2014.

[13] Fan Hong and Richard Blaikie. Plasmonic lithography: recent progress. *Advanced Optical Materials*, 7(14):1801653, 2019.

[14] Xiaohua Huang and Mostafa A El-Sayed. Plasmonic photo-thermal therapy (pptt). *Alexandria journal of medicine*, 47(1):1–9, 2011.

[15] Jakob Søndergaard Jensen and Ole Sigmund. Topology optimization for nano-photonics. *Laser & Photonics Reviews*, 5(2):308–321, 2011.

[16] Josep Miquel Jornet and Ian F Akyildiz. Graphene-based plasmonic nano-antenna for terahertz band communication in nanonetworks. *IEEE Journal on selected areas in communications*, 31(12):685–694, 2013.

[17] Jin Woo Lee and Yoon Young Kim. Topology optimization of muffler internal partitions for improving acoustical attenuation performance. *International journal for numerical methods in engineering*, 80(4):455–477, 2009.

[18] Shutian Liu and Heting Qiao. Topology optimization of continuum structures with different tensile and compressive properties in bridge layout design. *Structural and Multidisciplinary Optimization*, 43(3):369–380, 2011.

[19] Krister Svanberg. The method of moving asymptotesâa new method for structural optimization. *International journal for numerical methods in engineering*, 24(2):359–373, 1987.

[20] Eddie Wadbro and Martin Berggren. Topology optimization of an acoustic horn. *Computer methods in applied mechanics and engineering*, 196(1-3):420–436, 2006.

[21] Eddie Wadbro and Christian Engström. Topology and shape optimization of plasmonic nano-antennas. *Computer Methods in Applied Mechanics and Engineering*, 293:155–169, 2015.

[22] Eddie Wadbro and Christian Engström. Topology and shape optimization of plasmonic nano-antennas. *Computer Methods in Applied Mechanics and Engineering*, 293:155–169, 2015.

[23] Kentaro Yaji, Takayuki Yamada, Masato Yoshino, Toshiro Matsumoto, Kazuhiro Izui, and Shinji Nishiwaki. Topology optimization in thermal-fluid flow using the lattice boltzmann method. *Journal of Computational Physics*, 307:355–377, 2016.

[24] Hao Chi Zhang, Le Peng Zhang, Pei Hang He, Jie Xu, Cheng Qian, Francisco J Garcia-Vidal, and Tie Jun Cui. A plasmonic route for the integrated wireless communication of subdiffraction-limited signals. *Light: Science & Applications*, 9(1):1–9, 2020.

[25] Ji-Hong Zhu, Wei-Hong Zhang, and Liang Xia. Topology optimization in aircraft and aerospace structures design. *Archives of Computational Methods in Engineering*, 23(4):595–622, 2016.